Cluster Characteristics in a MIMO Indoor Propagation Environment

Nicolai Czink, *Student Member, IEEE,* Xuefeng Yin, *Member, IEEE,* Hüseyin Özcelik, Markus Herdin, Ernst Bonek, *Senior Member, IEEE,* and Bernard H. Fleury, *Senior Member, IEEE*

***Abstract*— Essential parameters of physical, propagation-based MIMO channel models are the fading statistics and the directional spread of multipath clusters. In this paper we determine these parameters in the azimuth-of-arrival/azimuth-of-departure (AoA/AoD) domain based on comprehensive indoor MIMO measurements at 5.2 GHz in a cluttered office environment using the SAGE algorithm for parameter estimation. Due to cluster identification in AoA/AoD-domain we found a greater number of clusters than those reported in previous publications. Regarding the fading statistics of clusters, so far not studied, strong (obstructed-)line-of-sight clusters show Rician fading, corresponding to few dominant propagation paths, whereas most clusters exhibit Rayleigh fading, corresponding to many paths with approximately equal powers and uncorrelated phases. Root-mean-square cluster azimuth spreads (CASs) were estimated with a novel method by appropriately restricting the support of the cluster azimuth distribution. We found that the estimated CASs are different when seen from transmitter or receiver, i.e. their ranges are from 2° to 9° and from 2° to 7° at the transmitter side and the receiver side, respectively.**

***Index Terms*— MIMO systems, radio propagation, multipath channels, modeling, clustering methods.**

I. Introduction

THE use of multiple antennas at both link ends (MIMO) in wireless communication systems promises high spectral efficiency and reliability. Accurate channel models are required for proper design of signal processing algorithms in the receivers of these systems and may also be used to gain insight into the propagation phenomena as such. An important feature of the MIMO propagation channel with respect to MIMO applications is the occurrence of multipath components (MPCs) in clusters. It is shown in [1] that channel models disregarding clustering effects result in overestimation of the channel capacity. In densely but homogeneously cluttered environments, the (root-mean-square) azimuth spread [2] and fading statistics are well-known commonly used quantities to assess the performance of smart antennas with low directional resolution (few antennas).

However, a global azimuth spread is not able to capture the detailed structure of direction dispersion in the radio propagation that is crucial for a number of MIMO transmission techniques, e.g. [3]. The following example demonstrates the need for a refined characterization of dispersion in azimuth of arrival (AoA) and azimuth of departure (AoD) where dominant clusters are described individually by their *cluster azimuth spreads* (CASs) [4]. Figure 1 shows two synthetic environments with different marginal one-dimensional azimuth power spectra. Scenario 1 (dashed line) shows one cluster with rather large CAS. Scenario 2 (solid line) exhibits two clusters with small CASs each. However, both scenarios *lead to the same global azimuth spread*. In this paper we therefore take the approach to characterise multipath clusters individually and investigate their CASs and their fading statistics. This approach extends the global view of overall fading statistics and a single angular spread for the environment.

A. Related work

Saleh and Valenzuela observed multipath clustering in the delay domain [5]. There are various definitions of "clusters" (e.g. [6], [7]). In our understanding a multipath cluster is a group of MPCs with similar propagation parameters, such as AoA, AoD, and delay.

In [8] and [9], experimental investigations showed that line-of-sight (LOS) scenarios exhibit Rician fading, while non-line-of-sight (NLOS) scenarios exhibit Rayleigh fading, which our results will confirm for *clusters*. The global angular spreads ranged between 30 and 70 degrees in the investigated environments. The authors of [10], [11] showed fading statistics for the 5 GHz and 2.4 GHz band. They evaluated Rician K-factors between 0.6 and 5.1.

Previous results on the characteristics of *clusters* were obtained mostly for single-input multiple-output (SIMO) channels where the MPCs are resolved in the AoA/delay-domain. Using the SAGE (Subspace Alternating Generalized Expectation-maximization) algorithm for estimating channel parameters, the authors of [6] investigated the distribution of cluster position, the distribution of MPCs' position per cluster, and the number of clusters and distribution of the number of

Manuscript received August 17, 2005; revised January 19, 2006 and November 15, 2006; accepted November 15, 2006. The associate editor coordinating the review of this paper and approving it for publication was C. Xiao. Part of this work was supported by the European-Commission-funded Network of Excellence NEWCOM. The Ph.D. of two of the authors was cosponsored by Elektrobit, Finland.

N. Czink and E. Bonek are with Vienna University of Technology, Institute of Communications and RF Engineering, Gusshausstraße 25/389, CG0414, Vienna 1040, Austria (e-mail: {nicolai.czink,ernst.bonek}@tuwien.ac.at).

N. Czink and B. H. Fleury are with Telecommunications Research Centre Vienna (ftw.), Donau-City-Straße 1, Vienna 1220, Austria (e-mail: {czink,fleury}@ftw.at).

B. H. Fleury and X. Yin are with Aalborg Univeristy, Fredrik Bajers Vej 7A, A3-202, Aalborg DK-9220, Denmark (e-mail: {bfl,xuefeng}@kom.aau.dk).

H. Özcelik is with McKinsey & Company, Herrengasse 1-3, Vienna A-1010, Austria (e-mail: Hueseyin_A_Oezcelik@mckinsey.com).

M. Herdin is with Rohde & Schwarz, Test and Measurement Division, Muehldorfstraße 15, Munich 81671, Germany (e-mail: markus.herdin@rohdeschwarz.com).

Digital Object Identifier 10.1109/TWC.2007.05595.

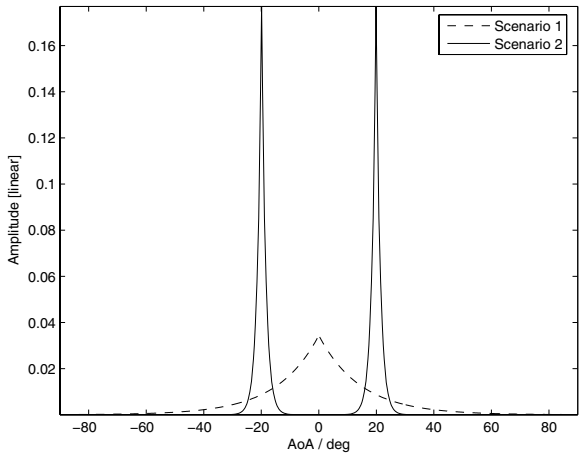

Fig. 1. Two exemplary angular power spectra leading to the same global azimuth spread equal to 20°.

MPCs per cluster. They found a mean number of 7 clusters in their scenarios. Using a spatial filter on SAGE estimates, [12] investigated the CAS and observed mean cluster angular spreads ranging between 6 and 36 degrees. (Note that these spreads are not rms values, but rather the extents of the clusters in the angular domain.) In [7], spreading parameters of the (assumed) Laplacian power spectrum of clusters were found to lie in the range from 21.5 to 25.5 degrees. The number of clusters and the average clusters rms angular spread was also investigated in [13]. The authors found an average number of only 2.3 clusters but rms CAS of 27 degrees by using the CLEAN algorithm.

B. Contributions

In this paper we provide insight into clustered wave propagation, and present *cluster* parameters, based on a comprehensive, well-documented MIMO measurement campaign in a cluttered office environment, which is characteristic for e.g. WLAN-MIMO deployment.

The detailed contributions of this paper can be summarized as follows:

- We introduce a more objective method for cluster identification in measurement data. The identification was carried out with an improved visual procedure using path estimates together with the double directional (AoA/AoD) power spectrum (APS), which shows better resolution than the AoA/delay domain.
- We introduce a new, more precise definition of what a cluster is, and restrict clusters by ellipses. Moreover, by choosing the sizes of the ellipses appropriately, the CAS estimator is nearly unbiased.
- Using the measurement data, we evaluated the CASs, where we found that they are different when seen from Rx and from Tx in our environment. We also found more clusters than in previous works, because of better resolution in the AoA/AoD domain. The evaluated CASs values can be used to parametrize the new cluster-based COST 273 MIMO channel model [14].
- Whereas fading statistics have been well investigated in literature, this contribution provides the first characterization of *cluster* fading to the best of the authors' knowledge. We found the intuitive result that NLOS clusters followed a Rayleigh distribution, but LOS clusters showed a Rician fading distribution.

C. Organisation

The paper is organized as follows. Section II describes the measurement equipment, and the indoor environment investigated during the channel sounding campaign. In Section III we introduce the methods for the cluster identification and cluster parameter estimation. The CASs and cluster fading statistics evaluated from measurements are presented in Section IV. We conclude in Section V.

II. Measurement

A. Measurement set-up

The measurements (see [15] for more details) were performed with the wideband vector channel sounder RUSK ATM [16] with a measurement bandwidth of 120 MHz at a center frequency of 5.2 GHz. At the transmit (Tx) side a sleeve antenna was mounted on a 2D positioning table. The antenna was positioned by means of two stepping motors controlled by the channel sounder. The Tx antenna was moved to 20 x- and 10 y-positions on a rectangular grid with mesh $\lambda/2$, forming a virtual 20×10 Tx planar array *without* mutual coupling. The receiver (Rx) was equipped with a directional 8-element uniform linear array (ULA) with 0.4λ inter-element spacing and two additional dummy elements. The antenna elements were printed dipoles on a backplane with 120° 3dB field-of-view. The elements were consecutively multiplexed to a single receiver chain.

For each position of the Tx antenna on the grid the channel sounder measured 128 successive snapshots of the frequency transfer function of the subchannel between the Tx antenna and each Rx antenna element. Within the measurement bandwidth of 120 MHz, 193 equidistant samples of the transfer function were taken. Altogether, each measured environment is represented as a $(128 \times 193 \times 8 \times 200)$ 4-dimensional complex channel transfer matrix containing the channel coefficients for each temporal snapshot, frequency, Rx and Tx position. Since the measurement of the whole 4-dimensional channel transfer matrix took about 10 minutes, we measured at night to ensure time-invariance. In a post-processing stage, all 128 temporal snapshots were averaged to increase the SNR. Furthermore the mutual coupling between the elements of the receiver array was numerically cancelled using the method proposed in [17]. For the following evaluations, we used only a sub-array of 12×6 Tx positions to mitigate large-scale fading effects.

B. Environment

The measurements were carried out in the offices of the *Institut für Nachrichtentechnik und Hochfrequenztechnik, Technische Universität Wien* with a map shown in Figure 2. In total, 24 Rx positions were investigated: one in a hallway with line-of-sight (LOS) to the Tx, the other 23 positions in

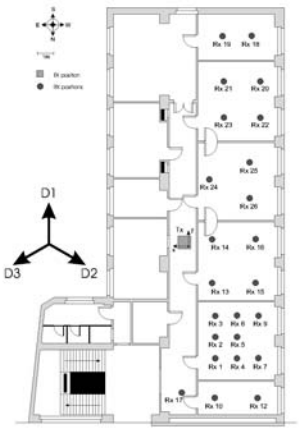

Fig. 2. Map of the investigated building with the Tx position and the various Rx positions.

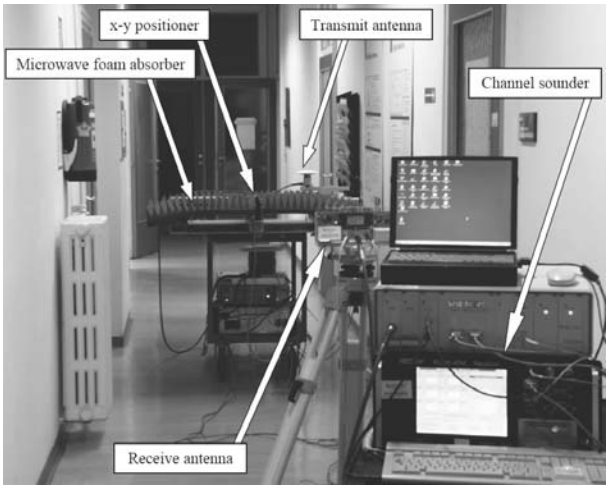

Fig. 3. Photograph showing the measurement equipment located in the corridor.

Fig. 4. Photograph of one Rx site in an office room (position Rx7D2).

various office rooms connected to this hallway with no-line-of-sight (NLOS) to the Tx. The location of the (virtual) Tx array was kept fixed in the hallway. Some rooms were amply, others sparsely furnished with wooden and metal furniture, bookshelves, and plants. Figures 3 and 4 show photographs taken with the equipment located in the corridor and an exemplary Rx scenario in one of the office rooms, respectively. At each Rx position, we rotated the Rx antenna to three different broadside directions D1, D2 and D3 as depicted in Figure 2. These directions were angularly spaced by $120°$. Thereby, we get 72 different measurement "scenarios", i.e. combinations of Rx positions and directions. The average coherence bandwidth of the measurements was around 5.8 MHz corresponding to 8 frequency bins [15].

In this paper we considered multiple realisations of 8×8 MIMO channels. Spatial realisations were generated by always considering all Rx antennas and forming a virtual ULA by grouping together measurement data collected at 8 adjacent Tx antenna locations [15, Ch. 4.3.3]. As the Tx virtual array has dimensions 12×6, by grouping the measurements collected at 8 adjacent antenna positions and using all 8 Rx antennas, we obtained $N_s = 30$ spatial realisations of the 8×8 MIMO channel matrix. Additionally all $N_f = 193$ frequencies were considered as realisations as well, which yields a total number of $N_f N_s = 5790$ channel realisations per measurement scenario.

III. Evaluation

We decided for estimating the cluster parameters in the AoA/AoD domain, as, in our case, this domain offers better separation of the paths than the angle/delay domain. Figure 5a shows an exemplary AoA/AoD power spectrum, whereas in Figure 5b the corresponding AoA/delay power spectrum is plotted. Even though using wideband measurements, the intrinsic delay resolution of 8.3 ns is too low for distinguishing clusters in indoor environments, while clusters are well separated in the angular domain.

To estimate the CASs and cluster fading statistics, we use the following steps: (i) Estimation of the parameters of the MPCs using the SAGE algorithm; (ii) Identification of clusters; (iii) Assignment of the estimated paths to the clusters; (iv) Estimation of the CASs and the fading statistics of each identified cluster.

A. Estimation of path parameters using the SAGE algorithm

For each measurement scenario, out of all 5790 channel realisations we randomly select a subset of $K = 150$ different channel realisations to keep the computational complexity tractable[1]. The 8×8 MIMO channel matrices are denoted by $\mathbf{H}^{(ij)}$ where i and j denote the indices of the frequency realisation and spatial realisation respectively, and $\mathbf{H}_k$ denotes the randomly chosen realisations, where $k = 1 \ldots K$.

Subsequently, we apply the SAGE algorithm [18] (implementation from [19]) to estimate the complex amplitudes, AoAs, and AoDs of the MPCs from each chosen channel

[1]We chose the realisations to be well separated over space and frequency to ensure low correlation between them.

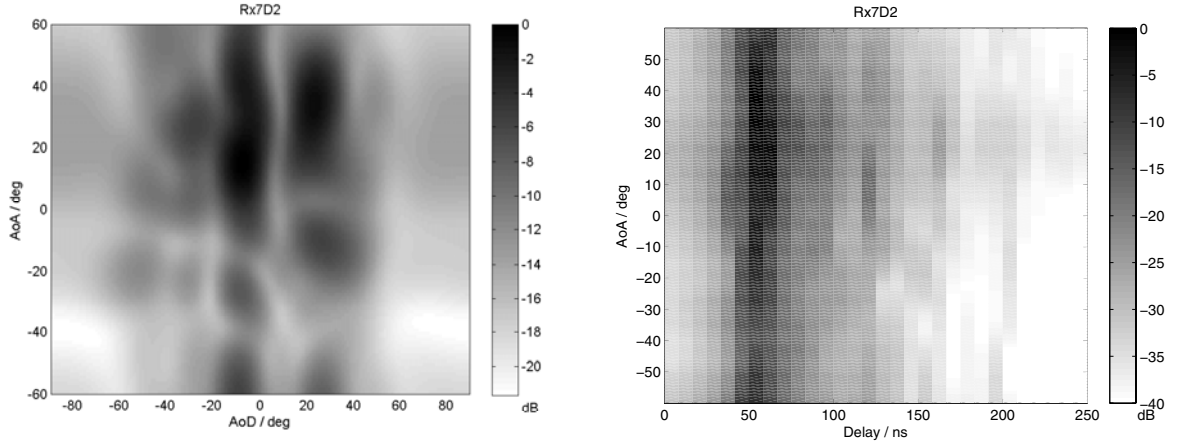

(a) (b)

Fig. 5. (a) Double-directional (AoA/AoD) power specturm, and (b) Delay/Angle-of-Arrival power spectrum computed from the same measurement data. Evidently, the delay resolution is not sufficient for cluster identification, while clusters can be clarly distinguished in the double-directional power spectrum.

realisation $\mathbf{H}_k$. The signal model used for the algorithm is the specular path model given by

$$\mathbf{H} = \sum_{p=1}^{N_p} A^{(p)} \mathbf{a}_{\mathrm{Rx}}(\varphi_{\mathrm{Rx}}^{(p)}) \mathbf{a}_{\mathrm{Tx}}^{H}(\varphi_{\mathrm{Tx}}^{(p)}), \tag{1}$$

where N_p denotes the number of paths, and the pth is described by its complex amplitude, $A^{(p)}$, and its AoA and AoD, $\varphi_{\mathrm{Rx}}^{(p)}$ and $\varphi_{\mathrm{Tx}}^{(p)}$, respectively. The normalized steering vectors of the respective arrays are denoted by $\mathbf{a}_{\mathrm{Tx}}(\cdot)$ and $\mathbf{a}_{\mathrm{Rx}}(\cdot)$, respectively.

SAGE estimation has to be performed conscientiously. The model order and the dynamic range have to be chosen carefully. The effective dynamic range of the measurements was at 55 dB. To be well within the SNR level of our measured channel realisations, we choose a dynamic range of 30 dB for the SAGE estimation. In order to extract as many paths as possible, the model order, i.e. the number of paths to be estimated, was selected to be maximum 49 in each realization. MPCs estimated with SNR below the dynamic range were discarded. With these settings we made sure that the dominant MPCs in the received signal were extracted.

The SAGE algorithm provides approximate maximum-likelihood estimates of the path parameters as ordered sets $\underline{\hat{A}}_k$, $\underline{\hat{\varphi}}_{\mathrm{Rx},k}$, and $\underline{\hat{\varphi}}_{\mathrm{Tx},k}$ of the MPCs, for each considered channel realisation k, $k = 1, \ldots, K$. The set $\underline{\hat{A}}_k$ is given by

$$\underline{\hat{A}}_k = \left(\hat{A}_k^{(1)} \quad \hat{A}_k^{(2)} \quad \cdots \quad \hat{A}_k^{(N_{\mathrm{p},k})} \right), \tag{2}$$

where each of the sets contain $N_{\mathrm{p},k}$ (the number of resolved paths in the kth channel realisation) elements, at most 49 (corresponding to the model order). The sets $\underline{\hat{\varphi}}_{\mathrm{Rx},k}$, and $\underline{\hat{\varphi}}_{\mathrm{Tx},k}$ are defined similarly.

The three ordered sets are collected in a parameter set

$$\hat{\mathbf{\Theta}}_k = \left(\underline{\hat{A}}_k \quad \underline{\hat{\varphi}}_{\mathrm{Rx},k} \quad \underline{\hat{\varphi}}_{\mathrm{Tx},k} \right) = \mathrm{SAGE}(\mathbf{H}_k), \tag{3}$$

describing all resolved (estimated) paths for the kth channel realisation. In (3) $\mathbf{H}_k$ denotes the channel matrix of the kth realisation and $\mathrm{SAGE}(\cdot)$ represents the estimates returned by the SAGE algorithm.

As a further check on the validity of the SAGE estimates, we evaluated the residual power of the channel by $\|\mathbf{H} - \hat{\mathbf{H}}\|_{\mathrm{F}}^2 / \|\mathbf{H}\|_{\mathrm{F}}^2$, where $\mathbf{H}$ denotes the measured channel realisation and $\hat{\mathbf{H}}$ denotes the reconstructed channel from the SAGE estimates according to (1), and $\| \cdot \|_{\mathrm{F}}^2$ denotes the Frobenius norm. We found that the residual power was, on average, only 5.7% of the signal power.

B. Cluster identification

Throughout literature (e.g. [6], [12]) clusters are identified visually. Currently, conventional heuristic clustering algorithms are both very time consuming and are inadequate, in that they do not utilize the properties of wave propagation (e.g. path powers are neglected). Conventional spectral-based methods usually exhibit larger angular spreads than the true spreads due to the limited resolution of the array response. Some automatic methods rely on a probability density function (pdf) for the parametric characterization of angular dispersion of the clusters. Proposed candidate pdfs are Gaussian, Uniform, and Von-Mises [20], [21], [22], [23]. These methods are computationally complex, especially in the multi-dimensional case. Furthermore, when the underlying pdf is different from the true distribution, this mismatch may lead to poor estimation results.

In contrast, the method proposed in this paper exhibits lower computational complexity. Furthermore, it does not require the knowledge of the actual angular distribution, therefore it is applicable for arbitrary distributions.

While we adopt the visual clustering approach, we improve it by using the estimated double-directional angular power spectrum (APS) [24] *jointly* with the AoD and AoA estimates of MPCs obtained with the SAGE algorithm.

We use the following method for visual cluster identification. The full spatial correlation matrix $\mathbf{R}_{\mathbf{H}}$ is calculated by averaging the channel matrices obtained from all 5790 realizations:

$$\mathbf{R}_{\mathbf{H}} = \frac{1}{N_s N_f} \sum_{i=1}^{N_s} \sum_{j=1}^{N_f} \mathrm{vec}(\mathbf{H}^{(ij)}) \mathrm{vec}(\mathbf{H}^{(ij)})^H, \tag{4}$$

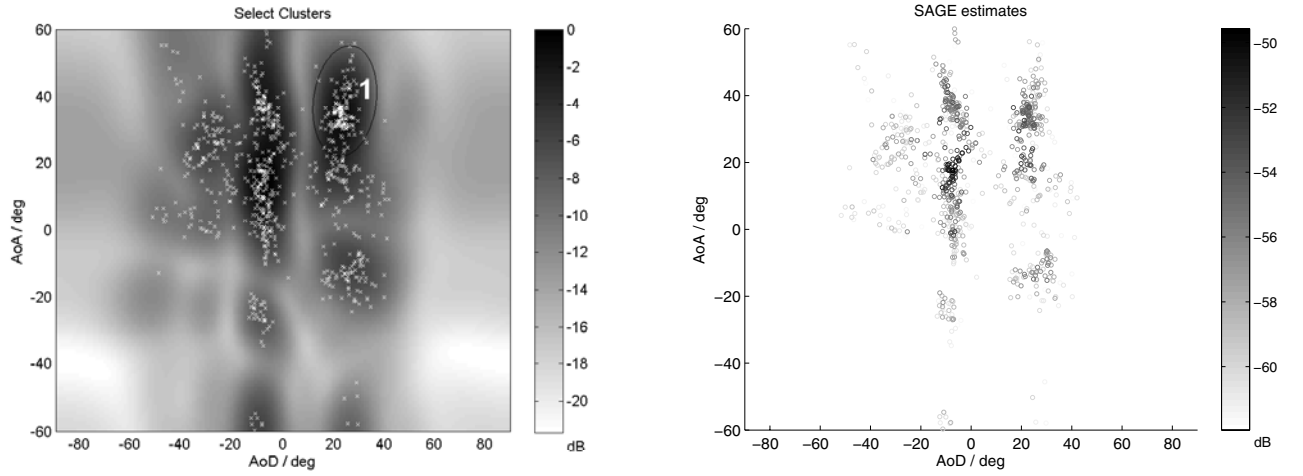

(a) (b)

Fig. 6. Visual cluster identification via the estimated APS (a) and the (AoA,AoD) estimates (b). The first already identified cluster is indicated by an ellipse.

where $(\cdot)^H$ denotes hermitian transpose, the $\mathrm{vec}(\cdot)$ operator stacks the columns of a matrix into a vector. By doing this, we partially cancel out small-scale and frequency selective fading effects.

The double-directional APS is estimated using the Bartlett beamformer [25]

$$P(\varphi_{\mathrm{Rx}}, \varphi_{\mathrm{Tx}}) = (\mathbf{a}_{\mathrm{Tx}}(\varphi_{\mathrm{Tx}}) \otimes \mathbf{a}_{\mathrm{Rx}}(\varphi_{\mathrm{Rx}}))^H \ \mathbf{R}_{\mathbf{H}} \ ((\mathbf{a}_{\mathrm{Tx}}(\varphi_{\mathrm{Tx}}) \otimes \mathbf{a}_{\mathrm{Rx}}(\varphi_{\mathrm{Rx}})), \quad (5)$$

where $\otimes$ denotes the Kronecker product.

In order to identify clusters in the AoA/AoD domain, we plot two figures: (i) the estimated APS (5), jointly with the (AoA,AoD)-pairs of 1000 paths exhibiting the largest gain amplitudes (Figure 6a); these paths are selected from all available path sets $\hat{\mathbf{\Theta}}_k$, and (ii) these pairs only in an AoA/AoD scatter plot, but colour-coded with a scale, indicating the gain amplitude (Figure 6b). Then we identify clusters by the following rules:

- Each "cluster" is defined as a group of MPCs showing similar AoA and AoD.
- In the scatter plot of (AoA,AoD) estimates, clusters show dense estimated MPCs with similar powers, where the powers of the MPCs decrease from the cluster's centre to the outskirts.
- In the APS the cluster power distribution must also decrease from the centre to the outskirts.
- Clusters must not overlap.

Using these rules, we can visually fit ellipses to match the clusters best. The elliptical shape is used for the following reason: in the AoA/AoD case, the power spectrum of a cluster can be described approximately using a pdf of the generalized Von-Mises-Fischer (VMF) distribution [26][2]. For small spreads, the contour lines of this distribution are close to ellipses.

[2]While this approximation has been a good working assumption for modelling multi-variate directional data, the VMF distribution has finally been found also in experiment [27].

Figure 6 demonstrates this approach applied to identify the first cluster for the exemplary scenario Rx7D2 (see floorplan in Figure 2). From Figure 6b, a clutter of AoD-AoA estimates can be observed, centered at approximately $(\mathrm{AoD}, \mathrm{AoA}) = (30°, 40°)$ with stronger power, the APS (Figure 6a) exhibits a (wide) peak there, too. The extent of the cluster is now estimated by fitting visually an ellipse to the AoA/AoD estimates. Notice that one has to take care that the cluster is not selected too large, since the estimated MPCs around $(\mathrm{AoD}, \mathrm{AoA}) = (30°, 15°)$ is likely to belong to another cluster, as one can see from the AoD-AoA scatter plot. This method is repeated, until all clusters of an environment are identified, i.e. there are no more significant MPCs to combine.

In the investigated Rx scenarios we find a mean number of 8.8 clusters within the field-of-view $(120°)$ of the Rx antenna. Note that we identified more clusters than observed in other comparative works [6], [7], [12]. The identified clusters have smaller angular spread in the AoA/AoD domain compared to those identified in the AoA/delay domain. The reason is that already small differences in delay may lead to clearly distinguishable AoDs, especially in indoor environments. In our case, the clusters can be more easily separated in the AoA/AoD domain than in the AoA/Delay or AoD/Delay domains. In this way, we increase the cluster resolution.

C. Cluster allocation

Characteristics of an identified cluster are gathered by using the AoA/AoD estimates allocated to this cluster. For this we determined to which ellipse each path belonged. This allocation is done for each scenario with the following algorithm.

For each cluster l, we allocated the SAGE estimates enclosed by the defined ellipse and collected them in cluster sets $\mathcal{C}_l$ by

$$\mathcal{C}_l = \left(\tilde{\mathbf{\Theta}}_{1l} \ \ \tilde{\mathbf{\Theta}}_{2l} \ \ \cdots \ \ \tilde{\mathbf{\Theta}}_{Kl}\right), \quad l = 1 \ldots N_c, \quad (6)$$

where N_c denotes the number of clusters in the considered scenario and $\tilde{\mathbf{\Theta}}_{kl}$ is a subset of $\mathbf{\Theta}_k$ containing the correspond-

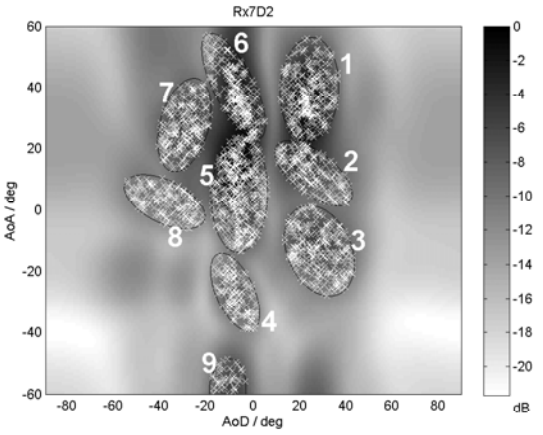

Fig. 7. Double-directional APS with identified clusters (ellipses) and allocated SAGE estimates (crosses) of the exemplary indoor scenario.

ing SAGE estimates for the considered cluster l and channel realisation k,

$$\tilde{\mathbf{\Theta}}_{kl} = \left(\underline{\tilde{A}}_{kl} \;\; \underline{\tilde{\varphi}}_{\mathrm{Rx},kl} \;\; \underline{\tilde{\varphi}}_{\mathrm{Tx},kl}\right), \quad \tilde{\mathbf{\Theta}}_{kl} \subset \hat{\mathbf{\Theta}}_k. \tag{7}$$

The indexed subsets $\underline{\tilde{A}}_{kl}$, $\underline{\tilde{\varphi}}_{\mathrm{Rx},kl}$, and $\underline{\tilde{\varphi}}_{\mathrm{Tx},kl}$ hold $N_{\mathrm{p},kl}$ (number of allocated paths in the kth realisation for the lth cluster) elements, each, and are again indexed as shown in (2). The sorting of the SAGE estimates into the cluster sets is done by geometrical considerations in the angular domain.

Figure 7 shows the double-directional APS obtained at the scenario Rx7D2 (see Figure 2). Identified clusters are enclosed by ellipses. AoA/AoD estimates falling within these ellipses are shown as white crosses. The sum powers of the paths within the clusters amount to 70% of the total estimated power on average. The other estimates can be interpreted as diffuse multipath and are discarded.

D. Cluster fading statistics

Once clusters are identified, their fading statistics and directional distributions can be determined.

To evaluate the cluster fading statistics we treat the channel as SISO channel using ideal omnidirectional antennas with propagation paths only from the respective cluster. All the paths are added coherently on this single antenna element. Doing this for many channel realisations results in fading.

It is common knowledge that high-resolution estimation of specular propagation paths in a cluster environment bears several risks. The model used for SAGE estimation assumes plane-wave propagation. This condition is not fulfilled in all scenarios. Scatterers can be very close to the Tx or Rx array. As a result wave-fronts may be curved. Since the underlying model does not account for these effects, the algorithm tries to approximate curved wave-fronts by multiple plane waves. Hence, seemingly resolved propagation paths might not exist.

Our algorithm for evaluating the fading statistics takes care of these effects by summing up fading contributions in the same channel realisation. So, paths estimated from one curved wave-front are treated as a single fading contribution.

To generate the fading realisations, we coherently sum the complex weights of the paths belonging to the same cluster and same realisation over n, $n = 1 \ldots N_{\mathrm{p},kl}$:

$$P_{kl} = \left| \sum_{n=1}^{N_{\mathrm{p},kl}} \tilde{A}_{kl}^{(n)} \right|, \quad k = 1 \ldots K, \tag{8}$$

where P_{kl} denotes the kth fading realisation in cluster l. For clusters with few significant paths, we expect the cluster to fade Rician, for clusters with equal-power paths we expect Rayleigh fading.

As there were only 150 fading realisations for each cluster, we have not been able to estimate Rician fading parameters, such as the K-factor, but we compared the resulting fading statistics to Rayleigh fading by conducting a Kolmogorov-Smirnov test [28]. This test provides a characterisation of the fading statistics, to be close to Rayleigh fading, below Rayleigh fading (e.g. double-Rayleigh), or above Rayleigh fading (e.g. Rician fading). "Above (Below) Rayleigh" is defined as a pdf whose mode[3] has a larger (smaller) value than the corresponding Rayleigh distribution with equal power.

Results for the considered scenarios are presented in Section IV.

E. Cluster azimuth spread

In this paper, we evaluate the rms *cluster* azimuth spread (CAS) using SAGE estimates based on the specular wave model. This approach extends the view of a global azimuth spread of the environment. Here, we restrict the investigations to the azimuthal dispersion.

One has to be careful with the estimation of the CAS. Due to our method using SAGE estimates based on the specular wave model, we only state a value of the rms CAS, and not a distribution function of the power within a this would yield demonstrably false results [29]. The reader is referred to this reference for the detailed explanation.

The *global* azimuth spread on one side, either Tx or Rx [2] is defined by the second order moment of the *azimuth power spectrum* at that side, which is given by

$$\varphi^{\mathrm{rms}} = \sqrt{\frac{\int_{-\pi}^{\pi} (\varphi - \bar{\varphi})^2 |A(\varphi)|^2 \mathrm{d}\varphi}{\int_{-\pi}^{\pi} |A(\varphi)|^2 \mathrm{d}\varphi}}, \text{ with } \bar{\varphi} = \frac{\int_{-\pi}^{\pi} \varphi |A(\varphi)|^2 \mathrm{d}\varphi}{\int_{-\pi}^{\pi} |A(\varphi)|^2 \mathrm{d}\varphi}, \tag{9}$$

where $|A(\varphi)|^2$ is the azimuth power spectrum of the considered scenario. In the case of the *cluster* azimuth spread (CAS) [4], only those components that contribute to the considered cluster have to be accounted[4]. For calculating the CAS, the power spectrum of the considered cluster $|A_l(\varphi)|^2$ has to be used.

We want to point out that a more accurate definition of the dispersion in the direction domain would be the *direction spread* [22], as this measure is more natural and moreover,

[3]The mode of a distribution is defined as the most probable value.

[4]Definition (9) is sometimes used, even when multiple large clusters are observed. As shown in Section I, in the case of a multiple-cluster environment this global directional spread fails to describe the directional dispersion of individual clusters.

relates to the stationarity region of the channel. However, for small values, the azimuth spread approximates the direction spread well. This especially applies to clusters, since the CASs are usually small.

For estimation of the CASs, we calculate the AoA and AoD rms CASs for each cluster l, by using the powers and angles of all resolved paths in the cluster. As the MPCs are assumed to be discrete, the integrals in (9) reduce to sums, so the mean AoA and AoD are separately estimated by

$$\bar{\varphi}_{\mathrm{AoA/AoD},l} = \frac{\sum_{k=1}^{K}\sum_{n=1}^{N_{p,kl}} \tilde{\varphi}^{(n)}_{\mathrm{Rx/Tx},kl}|\tilde{A}^{(n)}_{kl}|^2}{\sum_{k=1}^{K}\sum_{n=1}^{N_{p,kl}} |\tilde{A}^{(n)}_{kl}|^2}, \qquad (10)$$

and the rms CAS are obtained by

$$\hat{\sigma}_{\tilde{\varphi}_{\mathrm{AoA/AoD},l}} = \sqrt{\frac{\sum_{k=1}^{K}\sum_{n=1}^{N_{p,kl}} (\tilde{\varphi}^{(n)}_{\mathrm{Rx/Tx},kl} - \bar{\varphi}_{\mathrm{AoA/AoD},l})^2|\tilde{A}^{(n)}_{kl}|^2}{\sum_{k=1}^{K}\sum_{n=1}^{N_{p,kl}} |\tilde{A}^{(n)}_{kl}|^2}}, \qquad (11)$$

for each cluster l in the AoA (Rx) and AoD (Tx) domain.

Results for the considered scenarios will be presented in Section IV.

F. Accuracy of the CAS estimator

It has been shown in [29] that the azimuth estimates obtained by high-resolution parameter estimators based on the specular-path model exhibit a heavy-tailed distribution. The CAS estimator (11) computes the square root of the estimated second central moment of this distribution. The value of the CAS estimate computed using (11) increases along with the support range. This implies that the estimator can be biased when the support range is selected improperly. Therefore, a detailed study of the effect of the estimator is paramount. In the following we show by simulations that defining the clusters according to the rules given in Section III-B guarantees that the support is selected appropriately, and thus, the bias of the CAS estimate is reduced to a negligible amount.

In the simulations, channel matrices for an 8×8 MIMO system are randomly generated where the receiver and the transmitter are equipped with ULAs consisting of 8 isotropic antennas spaced by half a wavelength. For each scenario, N_c clusters are generated, where N_c is an integer randomly selected between 2 and 6. The nominal AoA and nominal AoD of the clusters are randomly selected in $[-60°, +60°]$ and $[-90°, +90°]$ respectively. To avoid heavily overlapping clusters, we disregarded samples where the nominal AoAs of any two clusters were spaced by less than $20°$.

Each individual cluster consists of L MPCs, where L is an integer randomly selected between 10 and 100. The AoAs and AoDs of the MPCs in each cluster are von Mises distributed random variables . The CASs $\sigma_{\tilde{\varphi}_{\mathrm{AoA}}}$ and $\sigma_{\tilde{\varphi}_{\mathrm{AoD}}}$ for individual clusters are randomly selected from the set $\{0.1°, 1°, 2°, \ldots, 8°\}$.

Two fading scenarios, i.e. Rayleigh and Rice fading, are considered in the simulations. For Rayleigh fading, the propagation paths have equal amplitudes and independent $[0, 2\pi)$-uniformly-distributed random phases. In the scenario with Rice fading, all propagation paths but a path located at the centre of the cluster, have equal magnitude and $[0, 2\pi)$-uniformly-distributed random phases. The dominant component has AoA and AoD equal to the nominal AoA and nominal AoD of the cluster respectively. The amplitude of this component is calculated to match the Rice factor and its phase is kept constant in all realizations of one simulation run. The Rice factor is the ratio between the power of the dominant component and that of the other components. In the simulation, we specify Rice fading only for clusters with CAS equal to $0.1°$ and use Rayleigh fading for clusters with larger CAS. This consideration is based on physical wave propagation, as clusters showing very small CAS can be considered as point sources or specular reflections. Thus, such clusters exhibit Rician fading. When the CAS is large, both Rice or Rayleigh fading scenarios are possible.

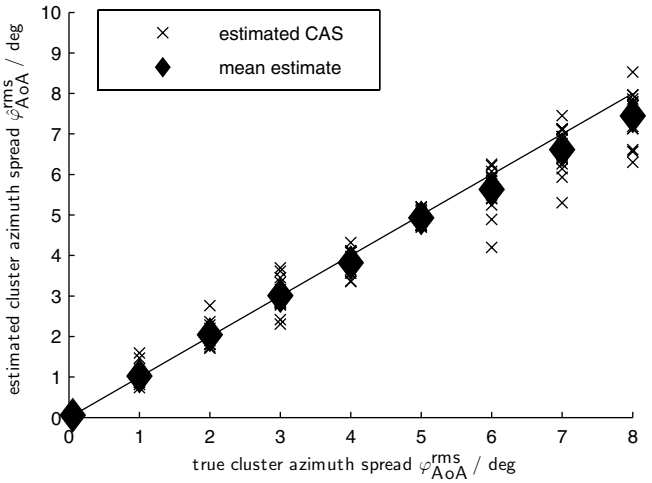

Fig. 8. Estimated CAS versus true CAS obtained in synthetic scenarios. Crosses indicate estimates for the different clusters, diamonds indicate the mean estimates. The estimator is nearly unbiased.

The signal-to-noise ratio (SNR) is defined as the ratio between the mean power of the received signals contributed by all clusters and the variance of the noise at each Rx antenna, and is set to 50dB.

We will present results for estimation of the CAS $\sigma_{\tilde{\varphi}_{\mathrm{AoA}}}$ only, as the estimator shows similar results for the CAS $\sigma_{\tilde{\varphi}_{\mathrm{AoD}}}$. Figure 8 illustrates the estimator performance for estimated CAS versus the true CAS. The CAS estimates are shown as crosses, the mean estimate is denoted as solid diamond. It can be observed that the estimated bias is positive when the true CAS less than $4°$, and negative for larger values. Since the absolute values of the biases are observed to be very small, the estimator is nearly unbiased, from a practical point of view, in the considered range.

The accuracy of the estimator is depicted in Figure 9, where the absolute errors, relative to the true value are plotted (crosses) together with their mean values (circles) and rms values (diamonds) for each distinct AoA. These errors are approximately 10% in average for $\sigma_{\tilde{\varphi}_{\mathrm{AoA}}} > 1°$, and larger than 20% for $\sigma_{\tilde{\varphi}_{\mathrm{AoA}}} < 1°$. This shows that the variance of the CAS estimator is sensitive to small CASs. However, since

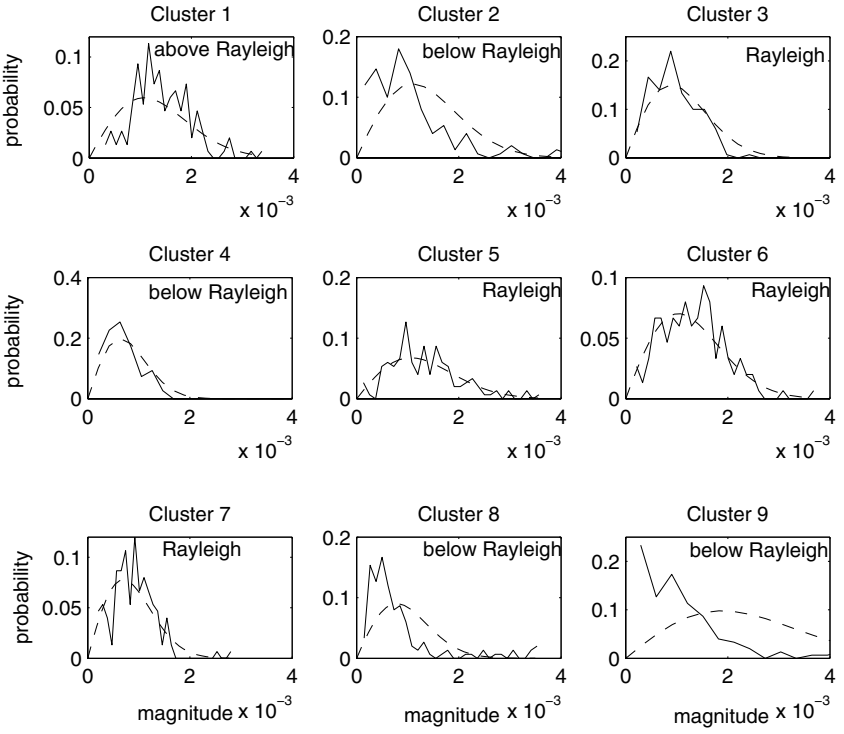

Fig. 10. Histrograms of the cluster amplitudes for the exemplary scenario (solid line) with fitted Rayleigh pdf (dashed line).

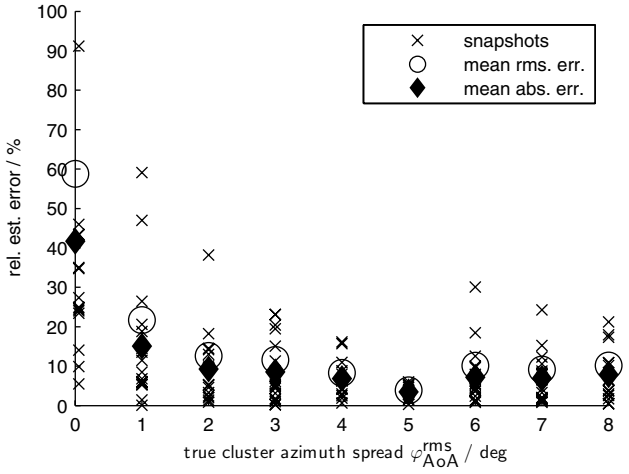

Fig. 9. CAS estimation errors in synthetic scenarios. The absolute errors relative to the true errors are evaluated for distinct cluster spreads. Crosses indicate estimates from the different clusters, circles the mean errors and diamonds the rms errors for the different cluster spreads.

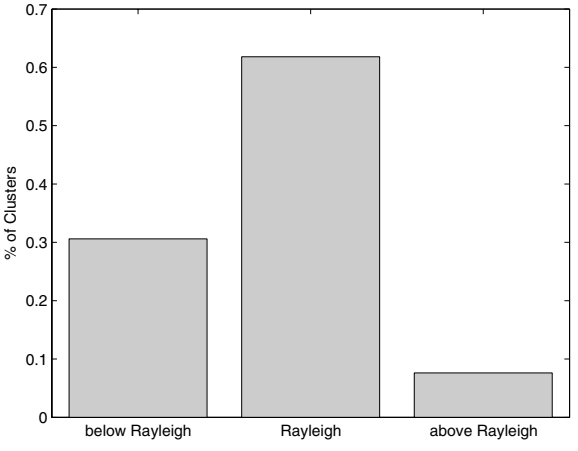

Fig. 11. Histogram of the three fading statistics "below Rayleigh", "Rayleigh", and "above Rayleigh"

the absolute error is small when $\sigma_{\tilde{\varphi}_{\mathrm{AoA}}} < 1^\circ$, from a practical point of view the estimates obtained with the true CAS less than 1° are acceptable.

IV. Results

A. Fading Statistics

Figure 10 shows the empirical fading pdf of (8) for each cluster l (solid lines) from the exemplary environment in Figure 7. For comparison, the Rayleigh pdf with equal power (black dashed line) are plotted.

In this example, cluster 1 exhibits prominent fading above Rayleigh. The other clusters either match Rayleigh fading or show too few estimates for further characterisation. Furthermore, in this scenario Cluster 1 corresponds to a obstucted-LOS path.

Fading above Rayleigh indicates the dominance of a few fading components. As expected, only clusters evolving from obstucted-LOS paths show prominent fading above Rayleigh.

The fading behaviour from all clusters is presented in

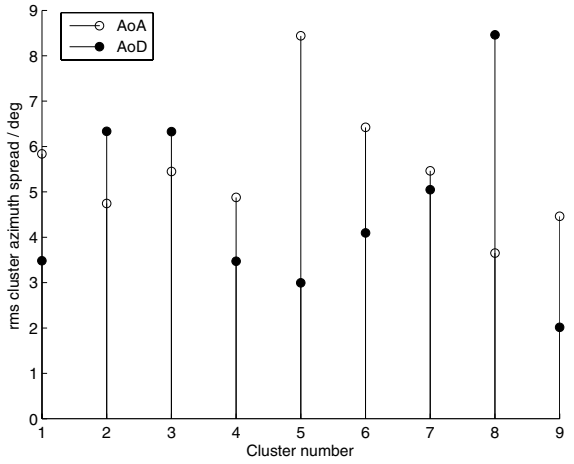

Fig. 12. CAS of individual clusters in the exemplary scenario evaluated for AoA and AoD

Figure 11. It shows a histogram of the results gained by the Kolmogorov-Smirnov test applied to all clusters, which decides on the fading behaviour. Clusters that are below Rayleigh fading are covered by too few paths and thus do not give sufficient information about their fading behaviour. We observe a large number of Rayleigh fading clusters (i.e. 390) and only a very small number of clusters showing fading statistics above Rayleigh (i.e. 48).

B. Cluster Azimuth Spreads

In Figure 12 the CASs for the previously considered environment (Figure 7) are shown.

Note that the CAS also depends on the size of the chosen ellipses defining the clusters. However, provided the cluster is defined following the rules described in Section III-B, the CAS does not change significantly with the size of the enclosing ellipse. This finding unhinges objections against insufficient precision in the process of defining cluster ellipses.

In Section III-F we showed that the proposed cluster spread estimator is nearly unbiased and shows only negligible estimation errors.

Table I details the number of clusters in each scenario and the mean CAS for all considered scenarios[5]. We observe an interdependence between the cluster parameters. When we identify a large number of clusters, their CASs are usually small and vice versa. Also, a large AoA CAS usually coincides with large AoD CAS.

A histogram of CASs obtained from all environments is shown in Figure 13. We usually observe larger AoA than AoD cluster spreads, as the transmitter was placed in a corridor. One can see that the AoA CASs mainly varies between 2 and 7 degrees, whereas the AoD cluster spread varies between 2 and 9 degree.

V. CONCLUSIONS

Multi-path clusters are characterised based on indoor measurements gathered in an office environment at 5.2 GHz.

[5]We kindly remind the reader of the 120° field-of-view of the Rx array.

TABLE I
CLUSTER PARAMETERS

Position	Number of clusters			AoA rms cluster azimuth spread in degrees (average)			AoD rms cluster azimuth spread in degrees (average)		
	D1	D2	D3	D1	D2	D3	D1	D2	D3
Rx1	5	12	9	7.9	6.0	4.7	3.4	3.8	4.6
Rx2	7	9	12	4.8	5.9	4.9	3.6	4.5	3.8
Rx3	6	13	9	4.7	5.0	5.0	5.2	5.2	4.5
Rx4	7	13	8	4.5	5.1	4.9	5.3	4.6	3.7
Rx5	6	14	9	4.7	5.0	5.5	5.4	5.0	4.3
Rx6	7	7	12	6.3	6.6	4.5	6.7	5.0	5.1
Rx7	8	9	7	4.8	5.5	5.8	4.7	4.7	3.7
Rx9	12	9	11	5.3	5.3	4.6	5.4	4.5	4.5
Rx10	9	10	11	5.0	5.7	4.7	4.6	3.6	3.9
Rx12	7	6	9	6.3	4.5	4.5	5.7	5.9	4.4
Rx13	7	7	7	5.3	6.9	6.1	5.8	7.1	5.4
Rx14	8	9	8	7.6	6.6	6.1	6.1	7.2	6.2
Rx15	8	7	9	7.6	6.0	5.5	8.4	8.8	6.9
Rx16	6	8	12	9.2	7.2	4.2	8.0	8.0	5.6
Rx17	7	7	6	4.4	4.3	8.2	3.9	5.1	5.6
Rx18	9	6	12	6.0	6.1	4.6	3.7	4.8	3.7
Rx19	5	6	11	6.2	6.5	4.4	6.5	4.5	3.3
Rx20	9	11	11	4.9	5.1	5.1	6.3	5.2	4.2
Rx21	12	9	6	5.2	6.6	6.4	4.2	5.2	4.9
Rx22	10	9	7	6.3	6.4	6.6	4.5	4.9	5.1
Rx23	8	9	9	6.5	6.9	5.4	5.1	5.8	5.1
Rx24	11	11	10	5.5	6.1	5.0	5.7	7.2	4.6
Rx25	5	10	11	7.0	4.9	4.7	8.2	5.3	6.0
Rx26	9	7	9	4.8	5.5	4.8	6.0	6.4	5.0
Average	8.8			5.5			5.2		

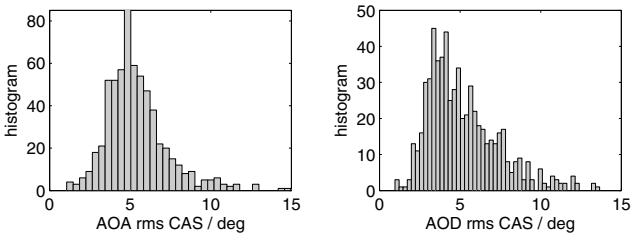

Fig. 13. Histogram of rms CAS over all scenarios (AoA domain left, and AoD domain right).

Clusters are evaluated for 72 scenarios with a subset of 150 realisations each.

To identify clusters, we propose an improved algorithm using the AoA/AoD power spectrum jointly with SAGE estimates. We introduce a new, more strict definition of what a cluster is, and restrict clusters by ellipses.

As we are considering the AoA/AoD-domain, the number of identified clusters is usually larger than in comparable publications. This fact becomes even more prominent as the Rx array had a limited field-of-view of 120°.

We investigate the cluster fading statistics, where we find that (obstructed-)LOS clusters show prominent Rician fading, whereas NLOS clusters exhibit Rayleigh fading.

To the best of the authors' knowledge, we did not find any comparative results on *cluster* fading in literature.

For the evaluation of the rms cluster azimuth spreads for the AoAs and AoDs, we introduced a novel estimator for the cluster angular spread which we found to be approximately unbiased and shows only negligible estimation errors.

As the transmitter was positioned in a corridor (providing

a preferred propagation path), we observe different cluster azimuth spreads in the AoD domain than in the AoA domain. We find the AoA rms azimuth spread mainly to range between 2–7 degree, the AoD rms azimuth spread between 2–9 degree. These results can be used to parametrize the new cluster-based COST 273 MIMO channel model [14]. Throughout literature, e.g. [6], [12], [7], [13], the azimuth spread was found to be much larger with a smaller number of clusters. The difference with the results presented in this paper results from our strategy of identifying clusters in the AoA/AoD domain instead of using the AoA/delay domain. Even a small, unresolvable deviation in the delay domain can result in completely different and well distinguishable AoDs. In the AoA/AoD domain multipath clusters can be separated more precisely. This explains why the estimated cluster spreads are smaller in our evaluation.

REFERENCES

[1] K. Li, M. Ingram, and A. Van Nguyen, "Impact of clustering in statistical indoor propagation models on link capacity," *IEEE Trans. Commun.*, vol. 50, no. 4, pp. 521–523, April 2002.

[2] P. Eggers, "Angular propagation descriptions relevant for base station adaptive antenna operations," *Kluwer Wireless Personal Commun.*, special issue on SDMA, vol. 11, pp. 3–29, 1999.

[3] M. Kiessling, J. Speidel, I. Viering, and M. Reinhardt, "Statistical prefiltering for MMSE and ML receivers with correlated MIMO channels," in *Proc. IEEE Wireless Communications and Networking Conference (WCNC '03)*, vol. 2, pp. 919–924.

[4] A. Kuchar, M. Tangemann, and E. Bonek, "A real-time DOA-based smart antenna processor," *IEEE Trans. Veh. Technol.*, vol. 51, no. 6, pp. 1279–1293, Nov. 2002.

[5] A. Saleh and R. Valenzuela, "A statistical model for indoor multipath propagation," *IEEE J. Sel. Areas Commun.*, vol. 5, no. 2, pp. 128–137, Feb 1987.

[6] C.-C. Chong, C.-M. Tan, D. Laurenson, S. McLaughlin, M. Beach, and A. Nix, "A new statistical wideband spatio-temporal channel model for 5-GHz band WLAN systems," *IEEE J. Sel. Areas Commun.*, vol. 21, no. 2, pp. 139–150, Feb. 2003.

[7] Q. H. Spencer, B. D. Jeffs, M. A. Jensen, and A. L. Swindlehurst, "Modeling the statistical time and angle of arrival characteristics of an indoor multipath channel," *IEEE J. Sel. Areas Commun.*, vol. 18, pp. 347–359, March 2000.

[8] J. Medbo, H. Hallenberg, and J. Berg, "Propagation characteristics at 5 GHz in typical radio–LAN scenarios," in *Proc. IEEE Vehicular Technology Conference 1999*, vol. 1, no. 49, pp.

[9] J. Medbo and J. Berg, "Spatio-temporal channel characteristics at 5 GHz in a typical office environment," in *Proc. IEEE Vehicular Technology Conference 2001*, vol. 3, no. 54, pp. 1256–1260.

[10] M. Carroll and T. Wysocki, "Fading characteristics for indoor wireless channels at 5 GHz unlicensed bands," in *SYMPOTIC'03*, pp. 102–105.

[11] T. Wysocki and H. Zepernick, "Characterisation of the indoor radio propagation channel at 2.4 GHz," *J. Telecommun. and Inf. Technol.*, vol. 1, no. 3–4, pp. 84–90, 2000.

[12] K. Yu, Q. Li, D. Cheung, and C. Prettie, "On the tap and cluster angular spreads of indoor WLAN channels," in *Proc. IEEE Vehicular Technology Conference Spring 2004*.

[13] A. S. Y. Poon and M. Ho, "Indoor multiple-antenna channel characterization from 2 to 8 GHz," in *Proc. IEEE ICC 2003*, vol. 5, pp. 3519–3523.

[14] L. Correia, Ed., *Mobile Broadband Multimedia Networks*. Academic Press, 2006.

[15] H. Özcelik, "Indoor MIMO channel models," Ph.D. dissertation, Institut für Nachrichtentechnik und Hochfrequenztechnik, Technische Universität Wien, Vienna, Austria, December 2004, downloadable from www.nt.tuwien.ac.at/mobile/theses_finished.

[16] R. Thomä, D. Hampicke, A. Richter, G. Sommerkorn, A. Schneider, U. Trautwein, and W. Wirnitzer, "Identification of time-variant directional mobile radio channels," *IEEE Trans. Instrum. Meas.*, vol. 49, pp. 357–364, April 2000.

[17] P. Lehne, F. Aanvik, J. Bic, P. Pajusco, M. Grigat, I. Gaspard, and U. Martin, "Calibration of mobile radio channel sounders," *COST 259, TD(98)088*, Duisburg, September 23–25, 1998.

[18] B. H. Fleury, M. Tschudin, R. Heddergott, D. Dahlhaus, and K. I. Pedersen, "Channel parameter estimation in mobile radio environments using the SAGE algorithm," *IEEE J. Sel. Areas Commun.*, vol. 17, no. 3, pp. 434–450, 1999.

[19] S. Semmelrodt, R. Kattenbach, and H. Früchting, "Toolbox for spectral analysis and linear prediction of stationary and non-stationary signals," *COST 273 TD(04)019*, Athens, Greece, January 26–28, 2004.

[20] O. Besson and P. Stoica, "Decoupled estimation of DoA and angular spread for spatially distributed sources," *IEEE Trans. Signal Processing*, vol. 49, pp. 1872–1882, 1999.

[21] T. Trump and B. Ottersten, "Estimation of nominal direction of arrival and angular spread using an array of sensors," *Signal Processing*, vol. 50, pp. 57–69, Apr. 1996.

[22] B. H. Fleury, "First- and second-order characterization of direction dispersion and space selectivity in the radio channel," *IEEE Trans. Inf. Theory*, vol. 46, no. 6, pp. 2027–2044, Sept. 2000.

[23] C. Ribeiro, E. Ollila, and V. Koivunen, "Stochastic maximum likelihood method for propagation parameter estimation," in *Proc. 15th IEEE International Symposium on Personal, Indoor and Mobile Radio Communications 2004*, vol. 3.

[24] M. Steinbauer, A. Molisch, and E. Bonek, "The double-directional radio channel," *IEEE Antennas Propag. Mag.*, vol. 43, no. 4, pp. 51–63, Aug. 2001.

[25] M. Bartlett, "Smoothing periodograms from time series with continuous spectra," *Nature*, vol. 161, 1948.

[26] K. V. Mardia, "Statistics of directional data," *J. Royal Statistical Society. Series B (Methodological)*, vol. 37, pp. 349–393, 1975.

[27] X. Yin, T. Pedersen, N. Czink, and B. H. Fleury, "Parametric characterization and estimation of bi-azimuth dispersion of path components," in *Proc. IEEE SPAWC 2006*.

[28] D. C. Boes, F. A. Graybill, and A. M. Mood, *Introduction to the Theory of Statistics, 3rd ed.* New York: McGraw-Hill, 1974.

[29] M. Bengtsson and B. Völcker, "On the estimation of azimuth distributions and azimuth spectra," in *Proc. IEEE Vehicular Technology Conference*, vol. 3, no. 54, pp. 1612–1615.

Nicolai Czink was born in Vienna, Austria, in 1979. He received the Dipl.-Ing. degree with distinction from Technische Universität Wien (TU Wien) in 2004. Since then he is pursuing his PhD as research assistant at the Institute of Communications and Radio-Frequency Engineering at TU Wien. In 2005 he additionally became junior researcher in the field of Wireless Communications at the Telecommunications Research Centre Vienna (ftw.).

Xuefeng Yin was born in Hebei, China, 1973. He received the B. S. degree in Optoelectronics from Huazhong University of Science and Technology, China, in 1995, and the M. S. degree in digital communications and the Ph.D. degree in wireless communications both from Aalborg University, Denmark, respectively, in 2002 and 2006. From 1995 to 2000, he worked in Motorola Cellular Infrastructure Cooperation, Hangzhou, China as a system engineer. Since August 2006, he has been an assistant professor in the Department of Electronic Systems, Aalborg University. His research interests are in sensor array signal processing, parameter estimation for radio channel, channel characterization, target tracking and identification in radar applications.

Hüseyin Özcelik was born in Vienna, Austria, in 1976. He received the Dipl.-Ing. degree in Electrical Engineering in 2001 (with highest honors) and the Dr. techn. degree in 2005 (with 'promotio sub auspiciis praesidentis rei publicae'), both from the Technische Universität Wien (TU Wien). From 2000 to 2005 he joined the Mobile Communications Group at the Institut für Nachrichtentechnik und Hochfrequenztechnik at the same university as a research engineer. He specialized in MIMO channel measurement and characterization. His field of interest is MIMO communications with a focus on the propagation side.

Markus Herdin works as a development engineer for signal processing and FPGA design at Rohde & Schwarz in the Test Systems for Wireless Network Optimization group. He received his Dipl. Ing. degree in mobile communications from the Vienna University of Technology, in 2001. He continued his research towards a Ph.D. in the mobile communications group at the Institute of Communications and Radio-Frequency Engineering, Vienna University of Technology. His research areas covered multiuser detectors for UMTS, mutual interference of Bluetooth and WLAN, MIMO channel measurements and MIMO channel characterization. After finishing his Ph.D. in 2004, he joined DoCoMo Communications Laboratories Europe GmbH, where he worked as senior researcher on MIMO multihop communication systems for 4G. Part of his work was the technical management of research projects on indoor MIMO propagation and multihop communication. In 2006 he changed from research to development and joined Rohde & Schwarz GmbH. He is now responsible for signal processing and FPGA design for coverage measurement devices.

Ernst Bonek was born in Vienna, Austria, in 1942. He received the Dipl.Ing. and Dr.techn. degrees (with highest honors) from the Technische Universität Wien (TU Wien). In 1984, he was appointed Full Professor of Radio Frequency Engineering at the TU Wien. His field of interest is mobile communications at large. Recent contributions concern smart antennas, the characterization of mobile radio channels, and advanced antennas and receiver designs. His group pioneered 3D superresolution measurements of the urban mobile radio channel, the "double-directional" viewpoint of the mobile radio channel, and propagation-based MIMO channel models. Previous fields of research were semiconductors, microwaves, optical communications, and intersatellite links. Altogether, he authored or co-authored some 170 journal and conference publications. He holds several patents on mobile radio technology. He co-authored the book *Data Transmission over GSM and UMTS* by Springer Verlag, and co-edited *Technology Advances of UMTS* by Hermes Scientific Publications. From 1985 to 1990, he served the IEEE Austria Section as a Chairman. From 1991 to 1994 he was a council member of the Austrian Science Fund, acting as speaker for engineering sciences. From 1996 to 1999 he served on the Board of Directors of the reorganized Post and Telekom Austria. He participated in the European research initiative COST 259 as chairman of the working group on Antennas and Propagation, and continued to serve in this position in COST 273. In URSI, he was chairman of Commission C "Signals and Systems" between 1999 and 2002. He is the initiator of ftw (Forschungszentrum Telekommunikation Wien), a public-private partnership for telecommunications research in Vienna, Austria. He was consultant/guest professor at ESA/ESTEC (Noordwijk, The Netherlands) in 1980/81, at TU Lulea (Sweden) in 1997 and with NTTDoCoMo (Yokosuka, Japan) in 2002.

Bernard H. Fleury received the diploma in electrical engineering and mathematics in 1978 and 1990 respectively, and the doctoral degree in electrical engineering in 1990 from the Swiss Federal Institute of Technology Zurich (ETHZ), Switzerland. Since 1997 Bernard H. Fleury has been with the Department of Communication Technology, Aalborg University, Denmark, where he is Professor in Digital Communications. He has also been affiliated with the Telecommunication Research Center, Vienna (ftw.) since April 2006. Bernard H. Fleury is presently Chairman of Department 2 "Radio Channel Modelling for Design Optimisation and Performance Assessment of Next Generation Communication Systems" of the on-going FP6 network of excellence NEWCOM (Network of Excellence in Communications). During 1978-85 and 1988-92 he was Teaching Assistant and Research Assistant, respectively, at the Communication Technology Laboratory and at the Statistical Seminar at ETHZ. In 1992 he joined again the former laboratory as Senior Research Associate. In 1999 he was elected IEEE Senior Member. Bernard H. Fleury's general fields of interest cover numerous aspects within Communication Theory and Signal Processing mainly for Wireless Communications. His current areas of research include stochastic modelling and estimation of the radio channel, characterization of multiple-input multiple-output (MIMO) channels, and iterative (turbo) techniques for joint channel estimation and data detection/decoding in multi-user communication systems.